NASA Contractor Report 3971

The Physical and Empirical Basis for a Specific Clear-Air Turbulence Risk Index

John L. Keller

CONTRACT NAS8-34687
APRIL 1986

NASA

NASA Contractor Report 3971

The Physical and Empirical Basis for a Specific Clear-Air Turbulence Risk Index

John L. Keller
University of Dayton Research Institute
Dayton, Ohio

Prepared for
George C. Marshall Space Flight Center
under Contract NAS8-34687

National Aeronautics
and Space Administration

**Scientific and Technical
Information Branch**

1986

TABLE OF CONTENTS

LIST OF FIGURES

LIST OF SYMBOLS

c_p	Specific heat at constant pressure
$\vec{F}$	Turbulent (subgrid-scale) momentum flux stress force
e	Total specific energy
g	Effective gravitational constant
H	Turbulent (subgrid-scale) diabatic heating rate
$\vec{i}$	Unit directional vector (eastward > 0)
$\vec{j}$	Unit directional vector (northward > 0)
$\vec{k}$	Unit directional vector normal to given horizontal surface (upward > 0)
N	Brunt-Vaisala frequency
R	Gas constant for dry air
Ri	Gradient Richardson number
Ri_{cr}	Critical (gradient) Richardson number
T	Atmospheric temperature
u	Eastward component of grid-scale wind
u'	Eastward component of subgrid-scale wind
v	Northward component of grid-scale wind
v'	Northward component of subgrid-scale wind
$\vec{V}$	Horizontal wind velocity vector
w	Vertical wind component
z	Geometrical altitude
α	Directional angle of horizontal wind vector
Δp	Pressure thickness of given atmospheric layer
ΔV	Magnitude of the horizontal velocity vector
$\Delta\theta$	Potential temperature thickness of well-defined turbulent layer (subscript 'L')
$\Delta\Theta$	Potential temperature thickness of meso-scale internal frontal layer (subscript 'M')
γ	$1/(1-K)$

ε	Total energy dissipation rate
Θ	Potential temperature
Θ'	Subgrid-scale component of potential temperature
κ	R/c_p
ρ	Density of air
ϕ	Geopotential height (gz)
$\underset{\sim}{\Phi}$	Grid-scale component of the diagnostic (gradient) Richardson number tendency
$\underset{\sim}{\varepsilon}$	Subgrid-scale component of the diagnostic Richardson number tendency
ψ	Montgomery stream function
∇	Horizontal or 'del' operator

FOREWARD

This report addresses the research which has been performed subsequent to that covered in NASA CR-3378: "Case Studies of Clear Air Turbulence Using the Diagnostic Richardson Number Tendency Formulation". The fundamental emphasis during both these efforts was to develop a technique which would be a significant improvement over those currently used for flight planning and avoidance of clear-air turbulence. Ideally, it should be both quantitative in determining its potential intensity and specific in the location of regions of relatively high risk. Furthermore, it should not rely on specialized data but be functional using the currently available raob (rawinsonde observation) system.

The encouraging results documented in the earlier report were considered compelling enough to warrant a closer look into the possibilities of a Specific Clear-Air Turbulence Risk (SCATR) index approach to the clear-air turbulence (CAT) problem. Unlike the aforementioned investigation, which considered the aspects of fuel conservation possible by avoiding sustained periods of flight in even light to moderate CAT, this study focuses on several cases of documented severe CAT. This was because commercial carriers and other potential users of such a SCATR index are concerned primarily with passenger and crew member safety.

This research was conducted by the University of Dayton Research Institute for the National Aeronautical and Space Administration, George C. Marshall Space Flight Center, under the technical direction of Mr. Dennis W. Camp and Mrs. Margaret

Alexander of the Systems Dynamics Laboratory. Part of the effort was performed at the Department of Geosciences, Purdue University. Portions of the research will be included in the author's Doctoral dissertation. The support for this effort was provided by Mr. A. Richard Tobiason of the Transport Aircraft, Aeronautical Systems Division, Office of Aeronautics and Space Technology, Contract No. (NAS8-34687). Support for the last year of effort was provided by Mr. David H. George of the Central Weather Processor project of the Program for Regional Observation and Forecasting Systems, Environmental Research Laboratories, National Oceanic and Atmospheric Administration.

The author wishes to thank Mr. Dennis Camp for his foresight in providing support for such a controversial approach to the CAT problem. Further thanks go to the Air Transportation Association, in particular Mr. Carl Knable of United Airlines, for their help and encouragement. Finally, thanks to Mr. James K. Luers and Mr. Patrick Haines of the University of Dayton Research Institute and Professors Phillip Smith and Win-Yee Sun of Purdue University for providing a sounding board for many of the concepts developed in this report.

SECTION 1

INTRODUCTION

Clear-air Turbulence (CAT) remains a troublesome problem for commercial, military and corporate aviation. This is in spite of the fact that the problem has been studied for over 25 years. As of 1977, the world-wide economic loss to aviation interests due to CAT exceeded $25 million annually (Hopkins, 1977). Because of the continued increase in air traffic, it is almost certainly much greater than that now. Hence, the need for improved operational CAT detection and forecasting techniques, particularly for severe CAT, continues.

CAT should actually be considered a generic term in that it represents turbulence occuring in statically stable shear layers which need not be cloud-free, but may contain nonconvective clouds. However, it does rule out the turbulence associated with convectively unstable planetary boundary layers (whether clear or not) and deep convection, such as thunderstorms, as well as mechanical turbulence due to wind flowing over the earth's surface.

The CAT phenomenon, as defined above, is most frequently found near the tropopause within jet stream/internal fronts associated with active extratropical cyclones. The relationship between layer thickness and vertical wind shear has been statistically related to the probable existence of turbulence within a given layer (e.g., Essenwanger and Reiter, 1969). Other observational studies have sought CAT in these regions as well as in the lower stratosphere (e.g., Dutton, 1969; Starr and Kemp, 1974; Reed and Hardy, 1972; Kennedy and Shapiro, 1975,80) in order to develop a picture of its relationship to both synoptic and meso-scale structures and dynamics. Theoretical (e.g., Lindzen and Rosenthal, 1976; Lalas and Einaudi,

1980) and empirical evidence (e.g., Parks et al., 1984; Hardy et al., 1973a) have both pointed to the association of CAT with Kelvin-Helmholtz (K-H) instabilities. The spontaneous development of K-H instabilities requires the existence within the layer of a critical gradient Richardson number, Ri_{cr}, where Ri is defined as

$$Ri = \frac{RT}{p\theta}\left(\frac{-\partial p}{\partial \theta}\right)\left|\frac{\partial v}{\partial \theta}\right|^{-2}$$

It has also become apparent that atmospheric gravity waves must play a supporting role in the development of K-H instabilities and their attendant turbulence by locally reducing Ri . The most frequent and well-known factor in the excitation of atmospheric gravity waves is significant terrain. One particular response to terrain has become known as "mountain waves" (Clark and Peltier, 1977; Smith, 1977). More recently there have been investigations into the role of organized convective systems, such as squall lines, as barriers to the mean flow; thus acting in much the same way as terrain to excite atmospheric gravity waves (e.g., Keller et al., 1983).

It has become apparent that CAT plays a significant role with respect to larger-scale dynamics. It acts as an internal sink of kinetic energy when viewed in terms of the large-scale circulation of the atmosphere (e.g., Schenk, 1974; Smith, 1980). While values of kinetic energy dissipation rates on a globally averaged basis are fairly small (perhaps 2 to 6 $W.m^{-2}$), they can be much larger for individual synoptic scale systems (e.g., Smith and Adhikary, 1974; Ward and Smith, 1976; Kung, 1977). Local concentrations of

CAT within turbulent shear layers at jet stream altitudes can produce dissipation rates more than an order of magnitude larger than the globally averaged values (e.g., Kennedy and Shapiro, 1975,80; Dutton, 1969).

A comprehensive discussion of the turbulent energetics of turbulent layers and their relationship to larger-scale structures is covered in Dutton (1971). A somewhat less mathematical review is contained in Hardy et al. (1973). Aside from its role as a dissipative mechanism, however, is the role CAT plays in generating potential vorticity. This aspect was studied by a number of workers in the early 1960s (e.g., Staley, 1960). More recent studies (e.g., Gidel and Shapiro, 1979; Holopainen and Nurmi, 1979; Shapiro, 1976, 1981) have more thoroughly investigated the intriguing implication that turbulent processes may actually drive the grid-scale dynamics in certain situations. This concept is similar to that advanced by Smith (1973) and Smith and Adhikary (1974) using kinetic energy budget analyses.

A discussion of the importance of CAT to aviation interests is included in Dutton (1971). Within the economic imperatives of that time the concerns were generally in terms of passenger and crew member safety and comfort. The advent of the "energy crisis" later in that decade added the additional concern of CAT's affect on aircraft fuel consumption (e.g., Winer and Wesler, 1981). In terms of flight planning, techniques for location and short-term forecasting of CAT for airline operations have remained quite primitive; relying on subjective "rules-of-thumb" and labor intensive meso-scale hand analyses (e.g., Hopkins, 1977; Keller, 1985).

There seems now to be a strong consensus within the aviation community that the CAT forecast currently provided by the NWS is not

adequate (Camp et al., 1980). Despite the great expense involved, most airlines which continue to support their own weather staffs create CAT forecasts independently of the NWS product. Those carriers which no longer have their own weather staff rely mostly on pilot reports (PIREPS) to give them some guidance. The decreasing volume of PIREPS and increasing number of airlines which are reducing or eliminating their weather support point to the need to develop an automated, quantitative, and specific CAT risk index which can, at least, act as a reliable forecasting tool to aid in flight planning.

SECTION 2

PHYSICAL BASIS

In this formulation CAT is viewed as a manifestation of internal, frictional dissipation of total energy following a parcel of air of unit area spanning a well-defined turbulent shear layer of potential temperature thickness $\Delta\theta$. The rate of total specific energy dissipation within the parcel, vertically integrated through $\Delta\theta$, can be shown (Roach, 1970) to be

$$\mathcal{E}_L = \begin{cases} \frac{(\Delta v)^2}{24} \Phi_L , & \Phi_L > 0 \\ 0 , & \Phi_L < 0 \end{cases} \qquad (1)$$

where in isentropic coordinates

$$\Phi = \left\{ -2 \left| \frac{\partial v}{\partial \theta} \right|^{-2} \left[\frac{\partial v}{\partial \theta} \cdot \left(\frac{\partial v}{\partial x} \cdot \nabla \right) v + \frac{c_p}{\theta} \frac{\partial v}{\partial \theta} \cdot \nabla T \right] + \nabla \cdot w \right\} , \qquad (2)$$

Δv is the magnitude of the horizontal vector wind difference through $\Delta\theta$, and an $L_{\text{subscripted}}$ variable is defined as:

$$( )_L \equiv \frac{1}{\Delta\theta} \int_{-\Delta\theta/2}^{+\Delta\theta/2} ( ) \, d\theta \, . \qquad (3)$$

A more thorough development can be found in the Appendix. The development in the Appendix is done using isentropic coordinates which yields somewhat cleaner derivations than the pressure coordinates used by Roach in his development. The use of isentropic coordinates has other benefits for this study; in particular, with respect to the analysis of the data to resolve the structure of internal fronts.

The quantity '$\bar{\Phi}_L$' represents the grid-scale forcing by larger-scale dynamical processes which are attempting to change the local gradient Richardson number, Ri_L, within a given layer. It is the grid-scale component of the so-called diagnostic Richardson number tendency (DRT) following the flow (see Appendix),

$$\frac{D}{Dt} \ln Ri_L = \begin{cases} -\bar{\Phi}_L & \text{no CAT} \\ -\bar{\Phi}_L - \bar{\mathcal{E}}_L & \text{CAT} \end{cases} , \quad (4)$$

where $\bar{\mathcal{E}}_L$ is the subgrid-scale component. Roach's fundamental assumption is that turbulence occurs within the layer as a response to these forces when they are acting to decrease Ri_L within the layer. Turbulence, then, works against these forces in order to maintain Ri_L at a small but nearly constant value. At least one recent observational study (e.g., Kennedy and Shapiro, 1975) has shown that the rate of energy dissipation is nearly equal to the rate at which the larger-scale deformation field, associated with the three-dimensional meso- and synoptic scale dynamics of the jet stream/frontal layers, is acting to increase the vertical shear within the layer. Since Ri_L is highly dependent on the vertical shear, this suggests that the basic assumption is not unreasonable. The equation relating ε_L and $\bar{\Phi}_L$ can be viewed as a transformation of the grid-scale energy contained within the larger-scale deformation field into turbulent energy, rather than acting to reduce Ri_L. No such relationship is assumed to be relevant to layers where these large-scale processes are attempting to increase Ri_L.

As individual parcels move along through the atmosphere they are acted upon by the constantly changing $\bar{\Phi}_L$ associated with these meso- and synoptic scale systems such that Ri_L, in the absence of CAT should increase and decrease according to $\bar{\Phi}_L$. However, the

fundamental assumption suggests that Ri_L, when averaged over meso- and synoptic time scales, would be observed to remain nearly constant within well-established turbulent shear layers provided that data of sufficient spacial and temporal resolution were available.

SECTION 3

APPLICATION USING ACTUAL DATA

Bosart and Garcia (1974) used a special analysis data-set in an attempt to calculate changes in Ri_L following the flow. Raob data were available with sufficient temporal resolution so that fields of Ri_L could be calculated at three-hour intervals. The vertical resolution was 2°K (50 - 200 m). Fields of Ri_L were then "predicted" three hours ahead using $\hat{\Phi}_L$ following hand analyzed parcel trajectories and compared to the Ri_L fields calculated using the actual analyzed data. Many trajectories were calculated for parcels which passed through strong baroclinic zones which likely contained layers of CAT.

Though they claimed good agreement between the predicted and the actual Ri_L fields, their results were severely criticized by Roach (1975). Roach contended that the claimed qualitative agreement between the observed and calculated Ri_L was highly questionable first by inspection and second because the contribution of subgrid-scale eddies, seen in the complete expression (4) for DRT and not included in $\hat{\Phi}_L$, can not be accounted for in the change of Ri_L when parcel trajectories pass through regions of turbulence. The accurate calculation of Ri_L following parcels requires very high resolution data in both space and time in the first place. When turbulence and other subgrid-scale eddies are acting to modify Ri_L, resulting changes in the detailed vertical structure of horizontal wind and potential temperature make defining particular turbulent shear layers virtually impossible.

From the above considerations it becomes clear why calculations of Ri_L following the flow are not likely to be useful. Why, then,

can it be expected that energy dissipation rates, based on the grid-scale forcing of Ri_L, be expected to provide useful information on the potential for CAT? The reason is simply a difference in the scale for which they are appropriately applied. Ri_L is a parameter which is highly sensitive to the vertical increment over which it is calculated. For a sufficiently detailed data set, calculations of Ri_L reveal the tendency for CAT to be correlated to small Ri_L values (< 1). Very high resolution data are required in order that the scale associated with CAT, for which Ri_L has meaning, can be resolved. On the other hand, the validity of $\bar{\Phi}_L$ is not restricted to data having very high resolution. Its basis is the role of the grid-scale dynamics in attempting to decrease grid-scale Ri. (Ri_M rather than Ri_L). It is reasonably assumed, then, that subgrid-scale shear layers, perhaps associated with gravity waves, and having smaller Ri (Ri_L) will necessarily decrease as well. Since the sublayers begin with smaller Ri_L they will reach Ri_{cr} well before the grid-scale layer ever could.

Indeed, Roach (1975) asserted that the directional variation of the horizontal wind vector through turbulent shear layers, associated with gravity waves would cause unacceptable errors in the evaluation of $\bar{\Phi}_L$. This is because even ultra-high vertical resolution wind data (such as Jimsphere/Jimsondes) is still not sufficient to resolve gravity waves in space and time to accurately calculate their contribution to the deformations contained in $\bar{\Phi}_L$ (e.g., Keller, 1981). Hence, while it is important that the data used to calculate $\bar{\Phi}_L$ be analyzed to accurately represent the details of meso-scale frontal zones, data fields should be smoothed sufficiently to eliminate spurious details.

The gridded data used for the calculations in this study came from raobs. These data were objectively analyzed on either pressure

surfaces (as in the case of NMC analysis grids) or isentropic surfaces (as in the case of the PROFS/CWP analysis grids) so as to maximize the resolution of the meso-scale frontal structure. Although gravity waves should be expected to influence the vertical structure of the horizontal wind field, particularly in strong vertical shear layers where CAT might be expected, analyses of raw raob wind profiles have revealed only minor directional variations through even the strongest shear layers. None of the quite extreme directional variations hypothesized in Brown's (1973) paper, in which he formulated a technique to correct for their existence when calculating Φ_L, have yet been observed when examining vertical profiles of horizontal wind from raw raob data. In addition, these data were smoothed in order to remove noise in the wind field that might cause potential problems in the calculation of Φ_L as discussed above.

However, energy dissipation rates calculated using data linearly fit through a meso-scale layer, Δn, will usually result in the smoothing or "blurring" effect which increases with increasing calculation increment. In his original paper Roach (1970) essentially attempted to correlate large values of Φ_M to pilot reports of CAT. Roach's case studies proved inconclusive. He attributed this largely to the poor vertical resolution of the forecast model output data and inadequate analysis data he was forced to use. This apparently lead to excessive smoothing of the "signal" and inconclusive correlations with CAT encounter reports. The data which will be used for this study had significantly greater vertical and horizontal resolution than that used by Roach (1970).

SECTION 4

RESULTS

Estimates of turbulent energy dissipation rates using (1) have been calculated for several cases of documented CAT. The documented CAT cases which were investigated include:

(1) Hannibal, MO accident	3,4 April 1981
(2) Wisconsin/Illinois outbreak	27,28 November 1984
(3) Appalacian range outbreak	5,6 February 1985

The first four sets of figures involve case study (1) which used hand-analyzed raob data. This case involved a well publicized encounter by a DC-10 with severe turbulence which occured at approximately 0135Z 04 April 1981 near 37 000 ft (225 mb) in the Hannibal, MO area. Figure 1 shows horizontal wind vectors and isotachs at 250 mb constructed using NMC analysis data. These data are available with only 50 mb resolution between 300 and 100 mb. While energy dissipation rates can be calculated using this relatively coarse resolution, it was of interest to investigate the effect of the vertical resolution of the horizontal wind field on the calculation of total energy dissipation rates for this case. To perform this study, raw raob wind sounding data were hand analyzed for a large region of the central U.S. in order to more realistically represent the vertical shear of the horizontal wind for the 50 mb layer centered at 225 mb.

Figure 2a compares the vertical structure of the horizontal wind between 300 and 100 mb at an NMC analysis data grid point (broken line) to that for a raob station (solid line; Amarillo,

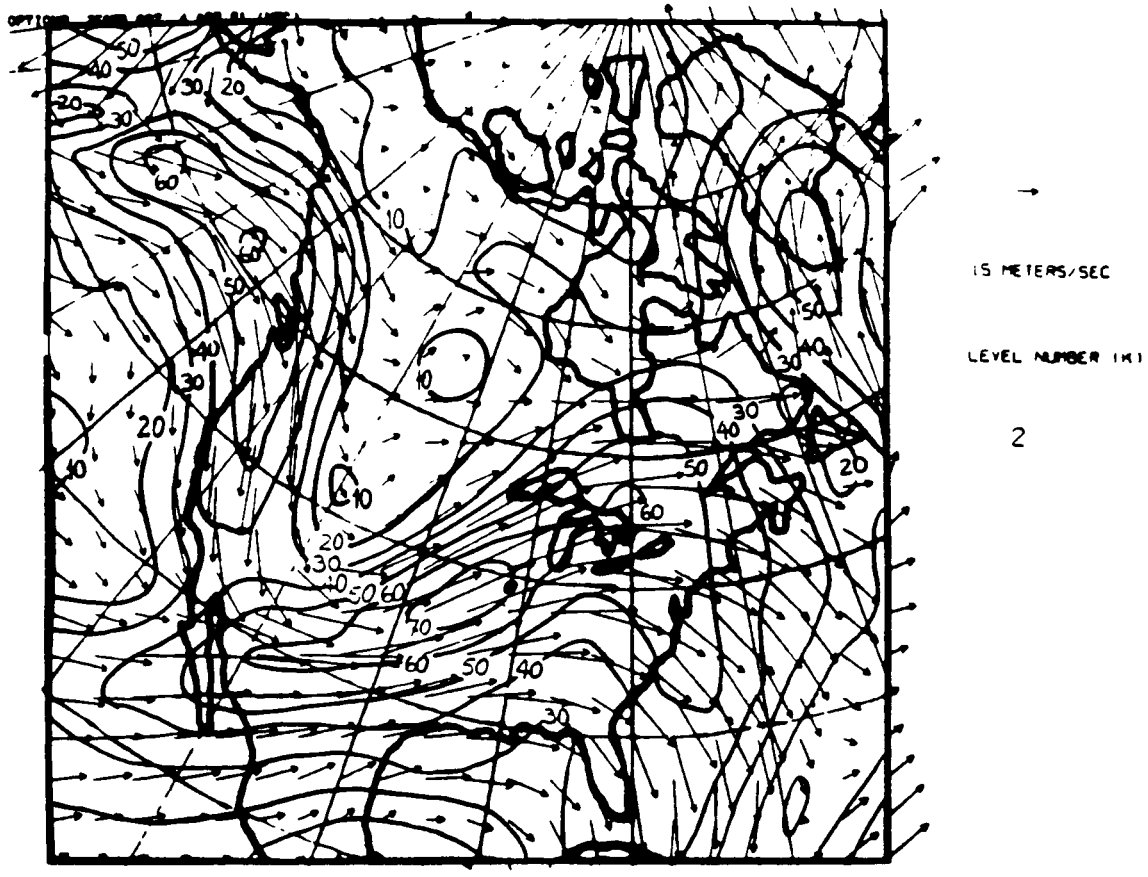

Figure 1 Horizontal wind vectors and isotachs (m/s) for 00Z 04 April 1981 at 250 mb.

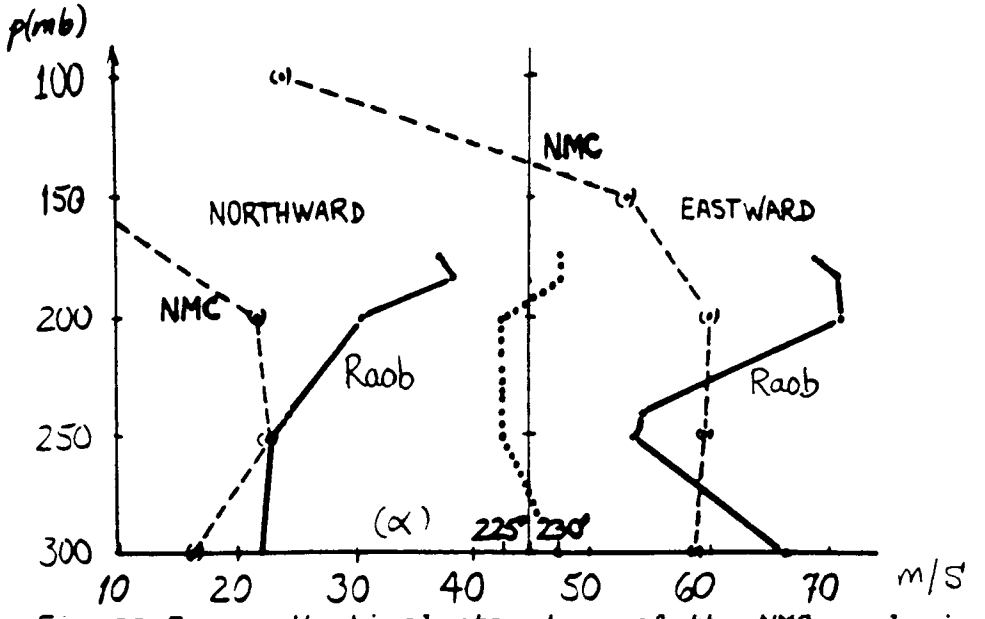

Figure 2a Vertical structure of the NMC analysis and raob horizontal wind components for an NMC grid point near a raob station for 00Z 04 April 1981. Dotted line, labeled α, shows the direction angle of the raob wind vector.

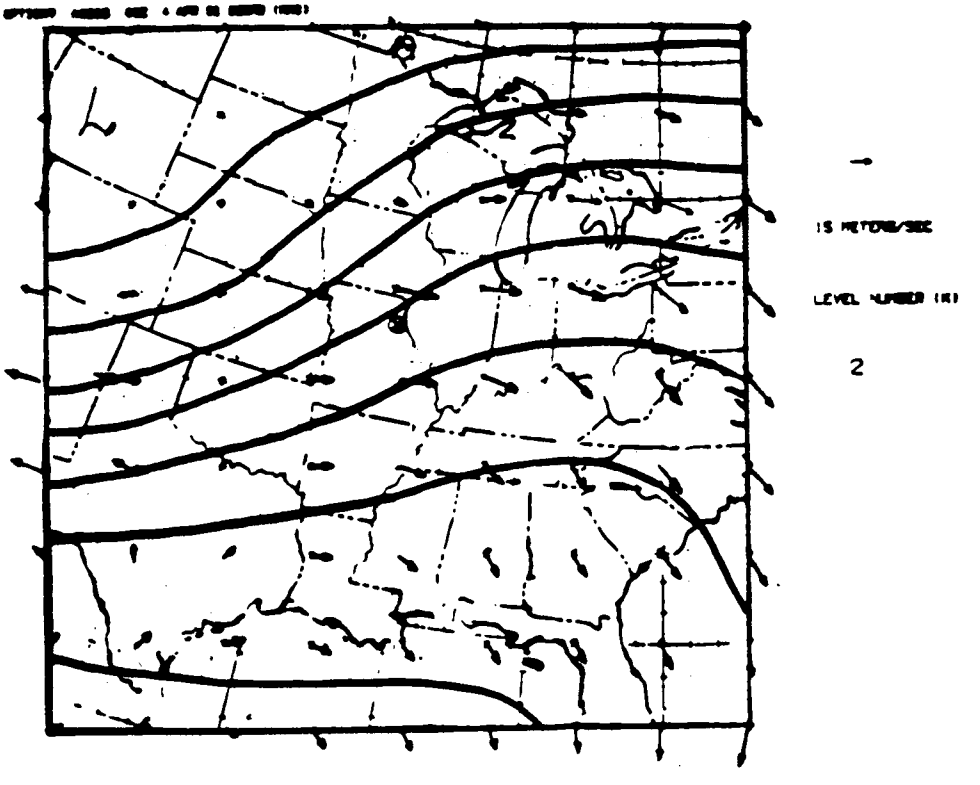

Figure 2b Horizontal ageostrophic vector wind field (NMC) for the 250-200 mb layer 00Z 04 April 1981.

TX) virtually at the same point. It can be seen that the analysis procedure greatly smoothes the shear in the horizontal winds. Also shown is the direction for the raob wind, α (dotted line). It is interesting to note that although the wind amplitude changes greatly through this range of altitude, the wind direction changes very little. The vertical shear of the horizontal wind is due almost entirely to changes in magnitude rather than direction. Inspection of numerous other raob wind profiles has shown that this behavior in the wind vector is by far the rule rather than the exception.

The methodology used in this case study was to reconstruct the horizontal vector wind field for the 225 mb level using the vertical shears for the 50 mb layer between 250 - 200 mb obtained from the raw raob profiles. It was the intent of this exercise to more approriately represent the vertical shear through the layer while preserving the nature of the horizontal wind field. Since the structure of the ageostrophic wind field is important in the evaluation of (1), it was felt that preserving this structure was evidence that the horizontal wind field had been reconstructed properly. Figure 2b shows the ageostrophic vector wind field calculated using the NMC winds. The circled 'x' indicates the approximate location of the CAT encounter. Figures 3a and 3b show for the NMC and raob winds the kinetic energy content, $1/2\ \mathbf{v}\cdot\mathbf{v}$ (heavy solid lines), and generation, $-\mathbf{v}\cdot\nabla\phi$ (thin solid lines). Energy content rather than specific energy per unit area were obtained by multiplying the specific kinetic energy values by $\Delta p/g$. It is clear that the horizontal structure of the reconstructed fields (raob) is very close to those for the NMC winds. Finally, figures 4a and 4b show the total energy content dissipation rates (heavy solid lines $x10^{-2}\ W\cdot m^{-2}$) which result using the NMC and the raob horizontal winds, respectively. In this case at least, a

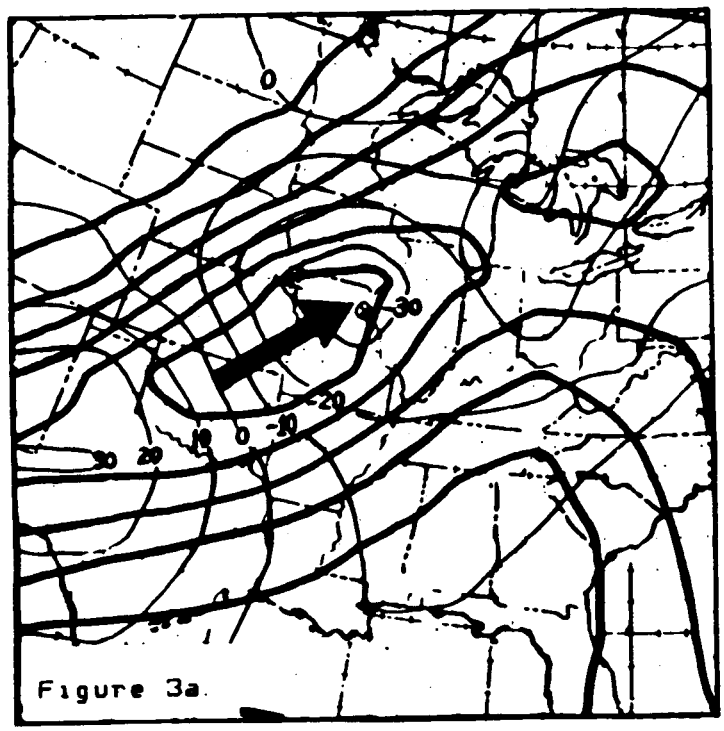

Figure 3a.

Kinetic energy content (heavy lines, $J \cdot m^{-2}$) and kinetic energy conversion (thin lines, $W \cdot m^{-2}$) for the 250-200 mb layer 00Z 04 April 1981 using NMC analysis data.

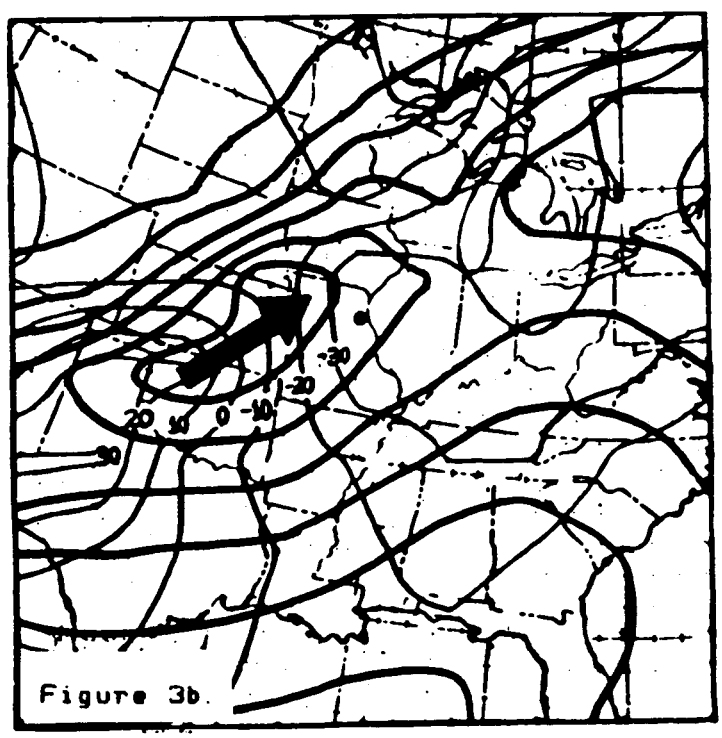

Figure 3b.

As 3a except using hand analyzed raob data.

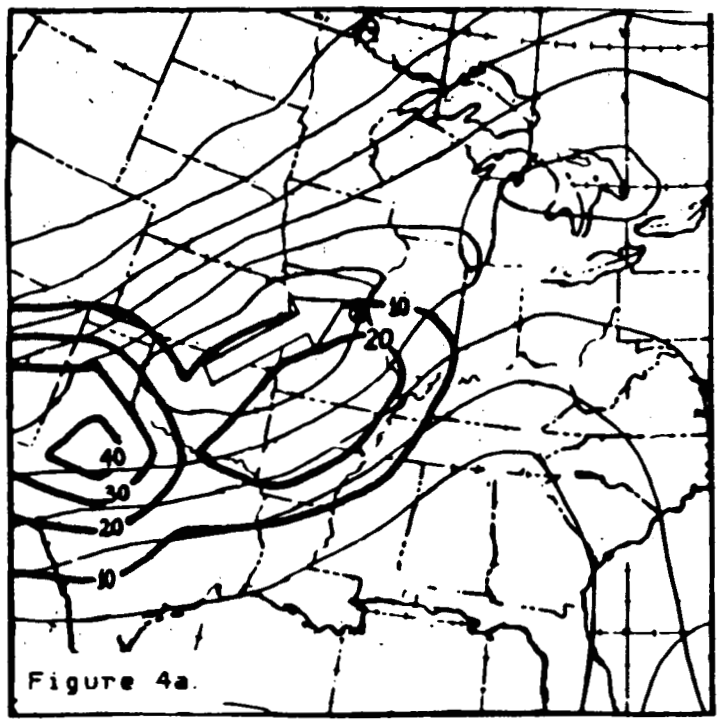

Figure 4a.

Total energy content dissipation rate (heavy lines, 10^{-2} W·m^{-2}) and kinetic energy content for the 250-200 mb layer 00Z April 1981 using NMC analysis data. The location of the CAT accident, at 225 mb, is indicated by the circled 'X'.

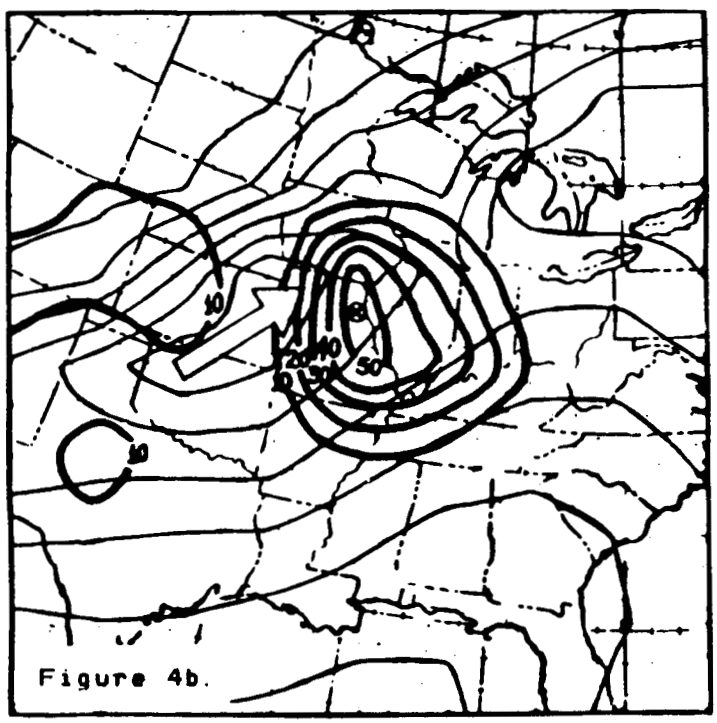

Figure 4b.

As 4a except using hand analyzed raob data.

more realistic representation of the vertical structure of the horizontal wind resulted in a dramatic change in the calculated total energy dissipation rate.

More recent calculations of specific energy rates have been performed using finer resolution PROFS/CWP grid point analysis data These data come from the standard raob network (North America) but have been analyzed to retain much of the detail lost during the NMC analysis procedure. These data were also analyzed on isentropic surfaces at PROFS/CWP. The horizontal grid is a stereographic projection with same geometry as that used by NMC; the resolution is about 75 km at mid latitudes. The vertical resolution starts out at 3°K around 700 mb and becomes 9°K near the tropopause level.

Figure 5 shows a measure of the total energy dissipation rate (actually, $\log\varepsilon_L$ + 7: Specific CAT Risk or "SCATR" index) calculated using 00Z 28 November 1984 analysis data for the 352 K surface. While not shown, there were pilot reports of CAT at this level over southern Wisconsin and northern Illinois near this time. There was also one reported over the state of North Carolina which may be associated with the area of large values of ε_L seen in the lower right-hand corner of the figure. The line running diagonally across the figure between the two 'x's corresponds to a hypothetical flight path between Omaha, NE and Detroit, MI. Figure 6 then shows the vertical cross-section of the SCATR index along this path.

Figure 7 shows the SCATR index field for 12Z 6 February 1985 at 25 000 feet. Locations of pilot-reported encounters with moderate to severe CAT occurred between 20 000 and 30 000 feet within two hours after 12Z are also shown. Figure 8 shows the

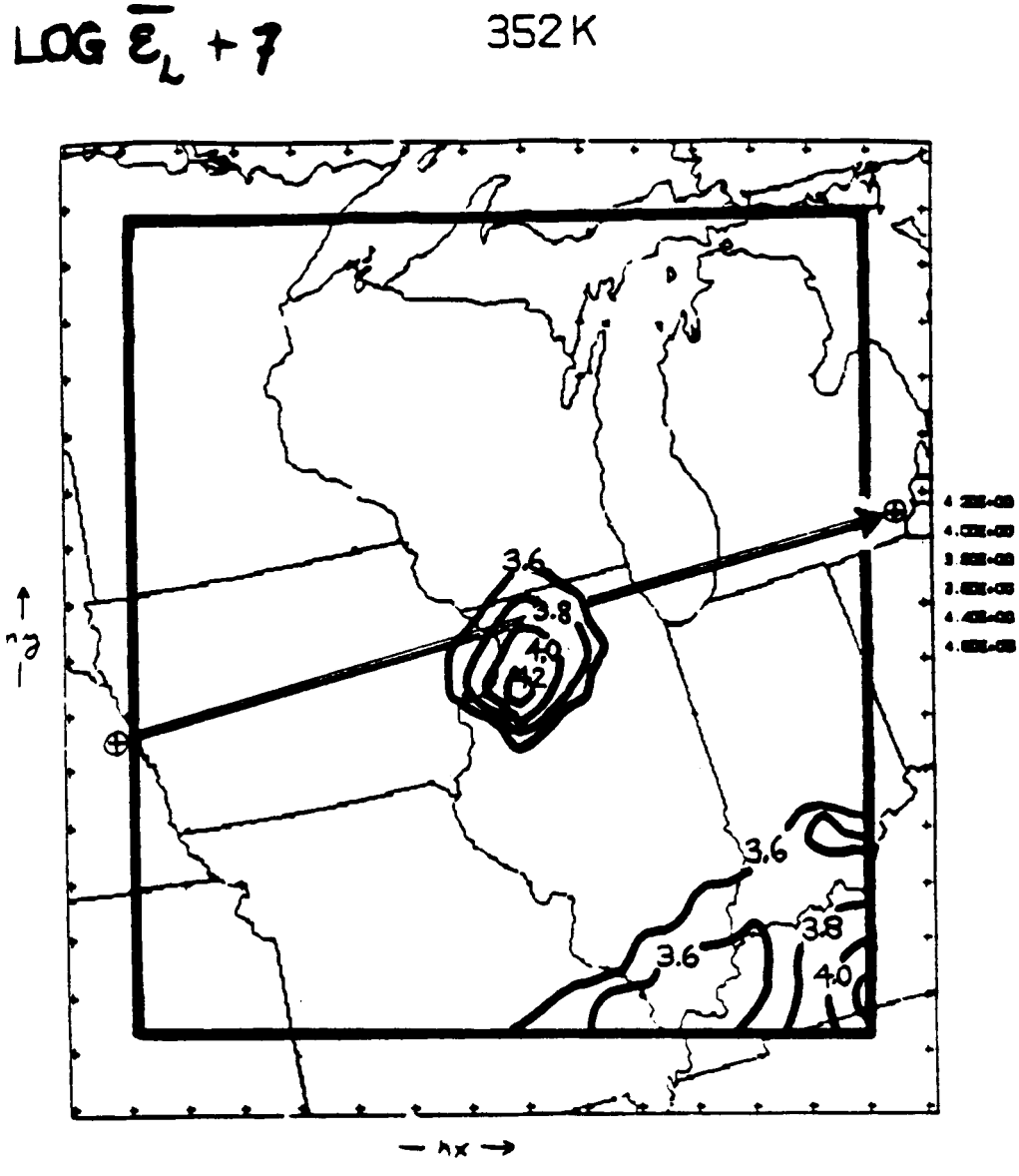

Figure 5. "SCATR index" on the 352 K potential temperature surface calculated using PROFS/CWP experimental isentropically analyzed raob data for 00Z 28 November 1984. The line running diagonally across the figure corresponds to a hypothetical flight path between Omaha, NE and Detroit MI.

ORIGINAL PAGE IS
OF POOR QUALITY

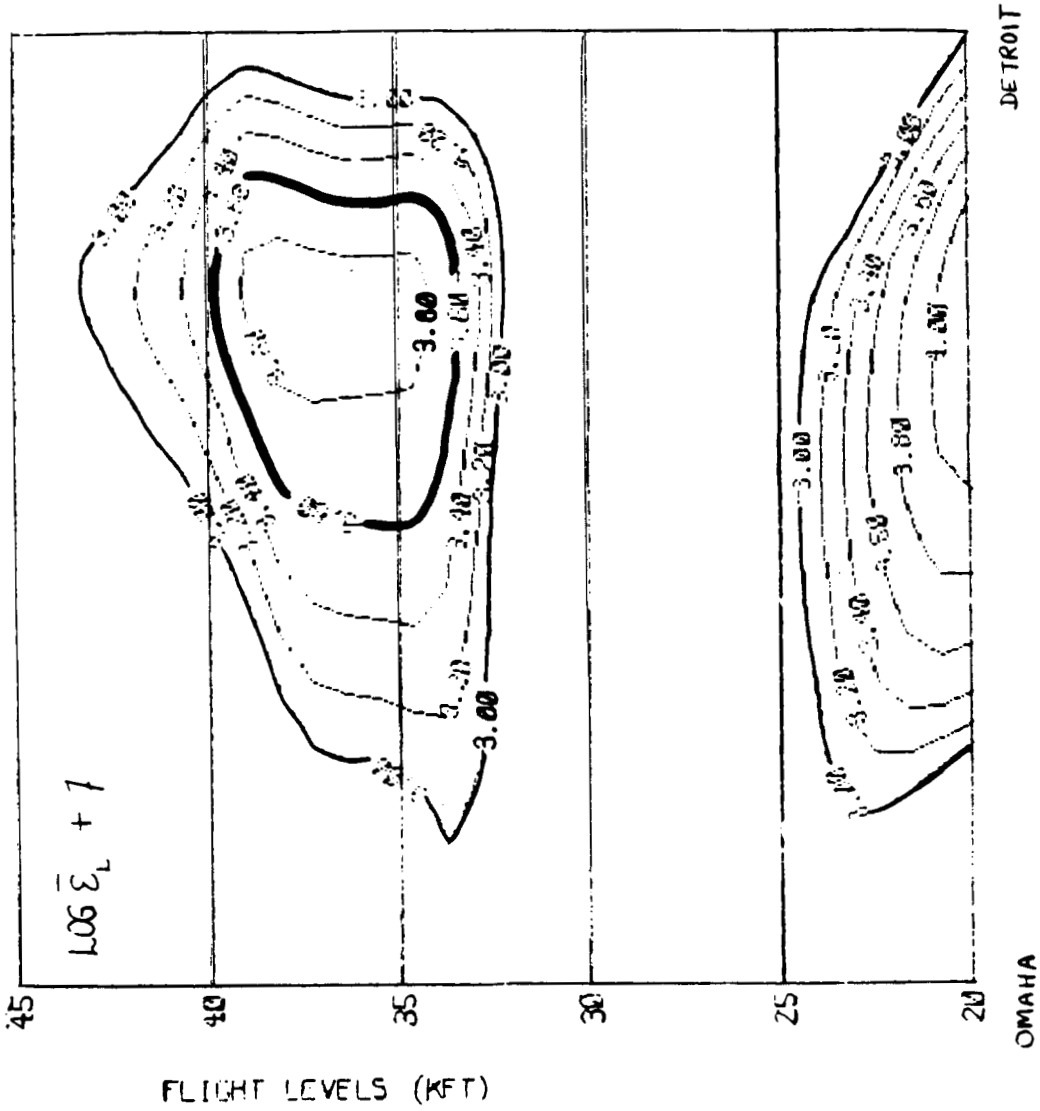

Figure 6. Vertical cross-section corresponding to the hypothetical flight path shown in figure 5

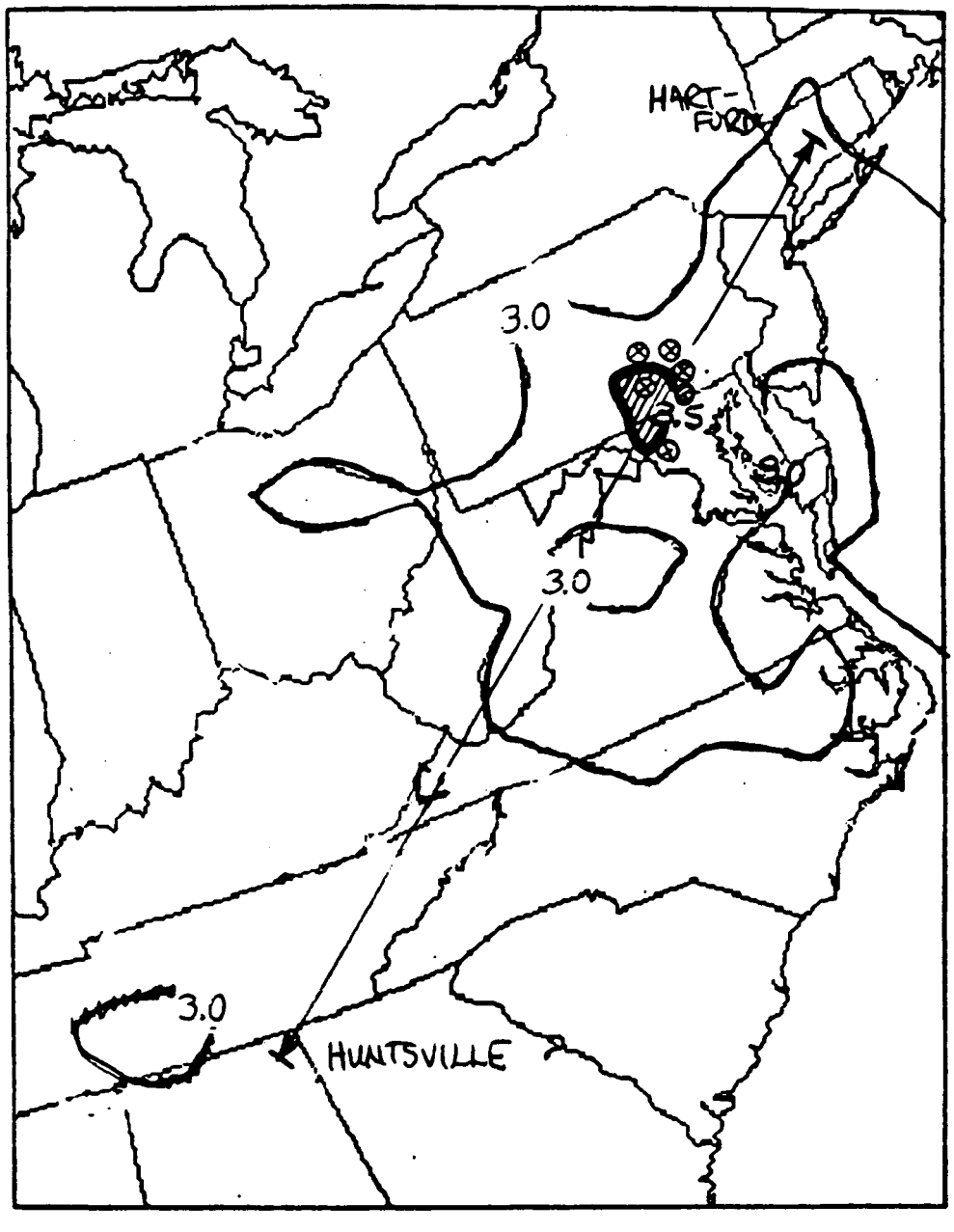

Figure 7. SCATR index field at 25 000 feet 12Z 06 February 1985 and moderate-severe CAT encounters reported near this altitude and time. The diagonal line represents a hypothetical flight path between Huntsville, AL and Hartford, CN.

vertical cross-section for the hypothetical flight path indicated by the line labeled by Huntsville and Hartford in Figure 7 along with the range of altitudes for which CAT was reported as well as smooth air reports.

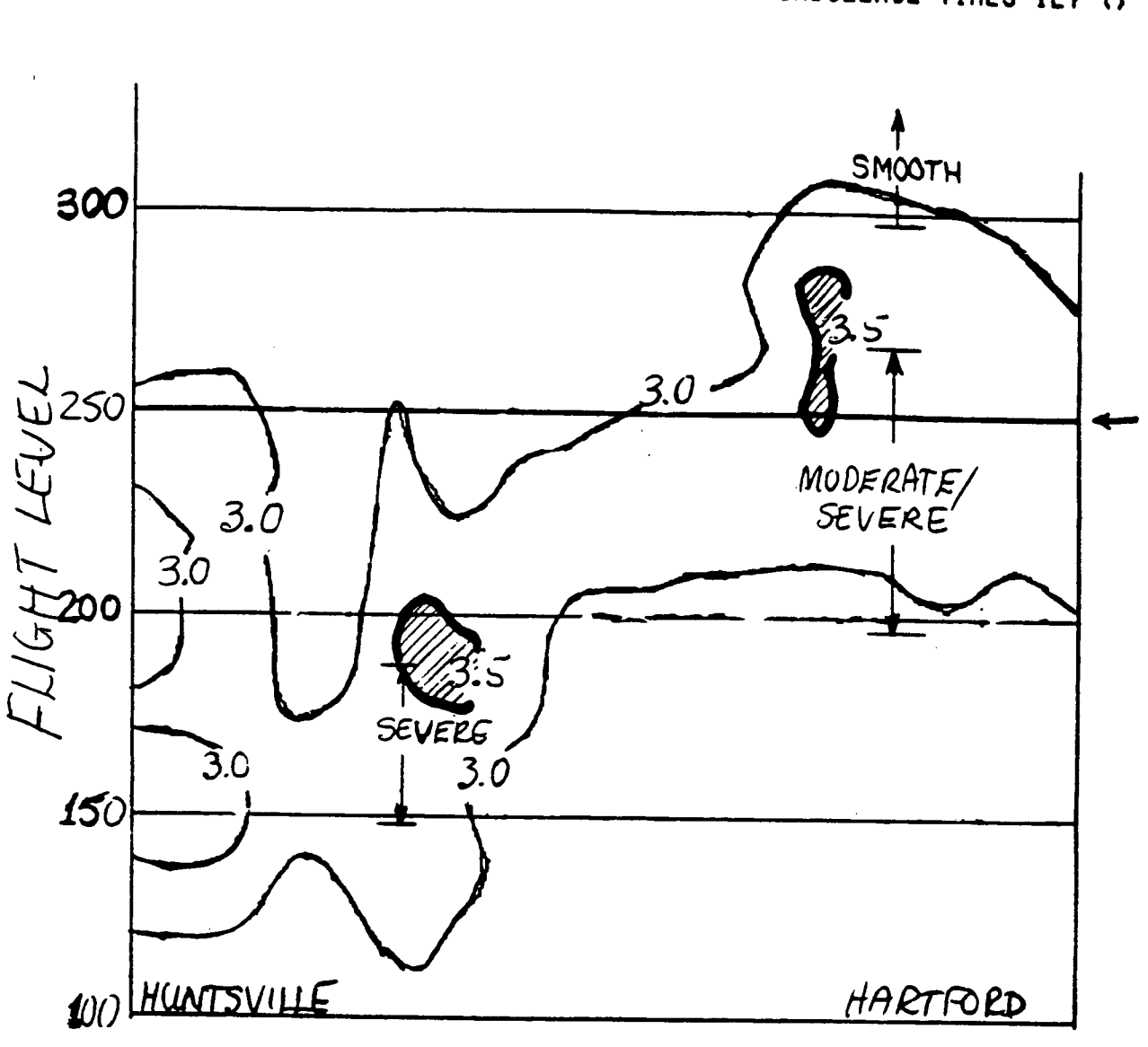

Figure 8. Vertical cross-section corresponding to the hypothetical flight path shown in Figure 7. Also shown are the altitude ranges and intensities of the reported CAT along this path.

SECTION 5

SUMMARY AND DISCUSSION

In summary, the SCATR index technique has shown some promising results. It seems apparent that the improvements seen in the case using hand analyzed data, as a result of the more realistic representation of the vertical shear of the horizontal wind, are also realized in the data analysis used in the PROFS/CWP application. Because of the important role of meso-scale processes in CAT formation, the performance of such a SCATR index should improve as database "enhancements", which will increase the resolution in both space and time, are brought into even more sophisticated objective analysis schemes. These enhancements include profiler and VAS satellite data as well as ASDAR and ACAR data.

The results of the case studies discussed above clearly suggest that a SCATR index is not an unrealizable goal. Uses of such an index, even in its current prototype level of development, are also apparent. These uses include the following:

(1) "Perfect prog" pseudo-forecasts of SCATR index fields could be generated taking advantage of the higher vertical resolution aviation forecast winds and temperatures (20 mb) soon to become available at NMC for 12 hour forecast intervals. This resolution is to be available between 300 mb and 100 mb.

(2) Fields of a SCATR index could be made available to NWS and other operational meteorologists who then could use it as a screening tool to determine which areas might be candidates

for applying meso-scale analysis techniques. Both perfect prog forecast and analysis SCATR index fields might be useful. Forecasters could then qualitatively account for the effects of significant terrain (mountain waves), organized convection, and other gravity wave sources

(3) Another application of such a SCATR index involves its use in generating self-consistent flight simulation databases. A number of flight scenarios could be created which match CAT patterns realistically to the wind and temperatures associated with any desired meteorological situation.

The above applications could be realized within a relatively short time; however, there are other applications for which such a SCATR index may be useful in the longer-term. These include:

(4) Use as part of a "MERIT" type short-term forecasting (or "nowcasting") model. This could be either by using forecasted variables, as for the perfect prog application above, or possibly by being incorporated as part of a parameterization for internal dissipation.

(5) The numerical values of a SCATR index provided by a nowcast model could then be used as input to flight path optimization programs. As mentioned in the introduction, CAT is known to produce aerodynamic penalties which increase fuel consumption. Passenger and crew member safety would also be improved in this way.

Of course, the best performance of a SCATR index would be realized if it is well-calibrated. In order to properly calibrate such an index, as well as more thoroughly validate and verify its

formulation, it is evident that a field study is necessary. During a field study the intensities determined from the grid-scale data given by (1) could be compared to the subgrid-scale intensities contemporaneously measured by experimental aircraft.

SECTION 6

REFERENCES

Bosart, L.F. and O. Garcia, 1974: Gradient Richardson number profiles and changes within an intense mid-tropospheric baroclinic zone. Quart. J. Roy. Meteor. Soc., 100, 593-607.

Brown, R., 1973: New indices to locate clear-air turbulence. Meteor. Mag., 102, 347-361.

Camp, D.W., W. Frost, E.M. Gross, J.F. Sowar, and A.R. Tobiason, 1980: Fourth annual workshop on meteorological and environmental inputs to aviation systems. Bull. Amer. Meteor. Soc., 61, 1628-1633.

Clark, T.L. and W.R. Peltier, 1977: On the evolution and stability of finite-amplitude mountain waves. J. Atmos. Sci., 34, 1715-1730.

Danielson, E.F., 1961: Trajectories: isobaric, isentropic and actual. J. Meteor., 18, 470-486.

Dutton, J.A., 1969: An energy budget for a layer of stratospheric CAT. Radio Sci., 4, 1137-1142.

_____, 1971: Clear-air turbulence, aviation, and atmospheric science. Rev. Geophys. and Space Sci., 9, 614-657.

Essenwanger, O.M. and E.R. Reiter, 1969: Power spectrum, structure function, vertical wind shear and turbulence in the troposphere and stratosphere. Arch. Meteor. Geoph. Biokl., Ser A, 18, 17-24.

Gidel, L.T. and M.A. Shapiro, 1979: The role of clear air turbulence in the production of potential vorticity in the vicinity of upper tropospheric jet stream-frontal systems. J. Atmos. Sci., 36, 2125-2136.

Hardy, K.R., M. Fukushima, P.F. Lester, and R.H. Stewart, 1973: On the prediction of turbulence in baroclinic zones. Boundary Layer Meteor., 5, 245-250.

_____, R.J. Reed, and G.K. Mather, 1973: Observation of Kelvin-Helmholtz billows and their mesoscale environment by radar, instrumented aircraft, and a dense radiosonde network. Quart. J. Roy. Meteor. Soc., 99, 279-293.

Holopainen, E. and P. Nurmi, 1979: Acceleration of a diffluent jet stream by horizontal sub-grid scale processes: an example of a scale interaction employing a horizontal filtering technique. Tellus, 31, 246-253.

Hopkins, R.H., 1977: Forecasting techniques of clear-air turbulence including that associated with mountain waves. WMO Tech. Note No. 155, 31pp.

Keller, J.L., 1981: Prediction and monitoring of clear-air turbulence: an evaluation of the applicability of the rawinsonde system. J. Appl. Meteor., 20, 686-692.

_____, 1985: Clear-air turbulence forecasting: towards a union of art and science. AIAA 23rd Aerospace Sciences Meeting, Reno, NV, 7pp.

Keller, T.L., L.J. Ehernberger and M.G. Wurtele, 1983: Numerical simulation of the atmosphere during a CAT encounter. Ninth Conf. Aerospace and Aeronautical Meteor., AMS. Omaha, NE.

Kennedy, P.J. and M.A. Shapiro, 1975: The energy budget in a clear-air turbulence zone as observed by aircraft. Mon. Wea. Rev., 103, 650-654.

_____, 1980: Further encounters with clear air turbulence in research aircraft. J. Atmos. Sci., 37, 986-993.

Kung, E.C., 1977: Energy sources in middle-latitude synoptic scale disturbances. J. Atmos. Sci., 34, 1352-1365.

Lalas, D.P. and F. Einaudi, 1980: Tropospheric gravity waves: their detection by and influence on rawinsonde balloon data. Quart. J. Roy. Meteor. Soc., 106, 855-864.

Lindzen, R.S. and A.J. Rosenthal, 1976: On the instability of Helmholtz velocity profiles in stably stratified fluids when a lower boundary is present. J. Geophys. Res., 81, 1561-1571.

Parks, E.K., R.C. Wingrove, R.E. Bach and R.S. Mehta, 1984: Identification of vortex induced clear-air turbulence using airline flight records. J. Aircraft, 22, 124-129.

Petersen, R.A., 1985: Three-dimensional objective analysis using a detailed isentropic cross-sectional procedure. Accepted by Mon. Wea. Rev.

_____ and L.W. Uccellini, 1979: The computation of isentropic atmospheric trajectories using a "discrete model" formulation. Mon. Wea. Rev., 107, 566-574.

Reed, R.J. and K.R. Hardy, 1972: A case study of persistent, intense clear-air turbulence in an upper level frontal zone. J. Appl. Meteor., 11, 541-549.

Roach, W.T., 1970: On the influence of synoptic development on the production of high-level turbulence. Quart. J. Roy. Meteor. Soc., 96, 413-429.

_____, 1975: Comment on paper 'Gradient Richardson number profiles within an intense mid-tropospheric baroclinic zone' by L.F. Bosart and O. Garcia. Quart. J. Roy. Meteor. Soc., 101, 392-393.

Schenk, H.A., 1974: A Simulation of the Influence of Clear Air Turbulence On the Large Scale Circulation of the Atmosphere. M.S. Thesis, Dept. of Meteorology, The Pennsylvania State University.

Sechrist, F.S. and J.A. Dutton, 1970: Energy conversions in a developing cyclone. Mon. Wea. Rev., 98, 354-362.

Shapiro, M.A., 1976: The role of turbulent heat flux in the generation of potential vorticity in the vicinity of upper-level jet stream systems. Mon. Wea. Rev., 104, 892-906.

_____, 1981: Frontogenesis and geostrophically forced secondary circulations in the vicinity of jet stream-frontal zone systems. J. Atmos. Sci., 38, 2642-2652.

Smith, P.J., 1973: The kinetic energy budget over North America during a period of major cyclone development. Tellus, 25, 411-423.

_____, 1980: The energetics of extratropical cyclones. Rev. Geophys. Space Phys., 18, 378-386.

_____ and S. P. Adhikary, 1974: The dissipation of kinetic energy in large-scale atmospheric circulations. Rev. Geophys. Space Phys., 12, 281-284.

Smith, R.B., 1977: The steepening of hydrostatic mountain waves. J. Atmos. Sci., 1634-1654.

Staley, D.O., 1960: Evaluation of potential vorticity changes near the tropopause and related vertical motions, vertical advection of vorticity, and transfer of radioactive debris from stratosphere to troposphere. J. Meteor., 17, 591-620.

Starr J.R. and B. Kemp, 1974: Meso-scale structure of jet streams and associated clear-air turbulence. Meteor. Mag., 103, 313-329.

Uccellini, L.W., P.J. Kocin, R.A. Petersen, H.W. Wash, and K.F. Brill, 1984: The President's Day Cyclone of 18-19 February 1979: Synoptic overview and analysis of the subtropical jet streak influencing the pre-cyclogenetic period. Mon. Wea. Rev., 112, 31-55.

Ward, J.H. and P.J. Smith, 1976: A kinetic energy budget over N. America during a period of short synoptic wave development. Mon. Wea. Rev., 104, 836-848.

Winer, D.E. and J.E. Wesler, 1981: Meteorological impact on aviation fuel efficiency. Proceedings of the Fifth Annual Workshop on Meteorologica and Environmental Inputs to Aviation Systems, NASA CR-2192, 15-20.

SECTION 7

APPENDIX

I. The Total Energy Dissipation Rate: Subgrid-scale Information from Grid-scale Data

This development will generally follow that of Roach (1970); however, there will be several deviations from his approach. The most significant deviation being the use of isentropic rather than pressure coordinates. The development will also show more detail than what was apparently possible in his paper.

The equations of motion in isentropic coordinates

$$\frac{D\mathbf{v}}{Dt} = \frac{\partial \mathbf{v}}{\partial t} + (\mathbf{v}\cdot\nabla)\mathbf{v} + H\frac{\partial \mathbf{v}}{\partial \theta} = -\nabla\psi - f\mathbf{k}\times\mathbf{v} + \mathbf{F} \tag{A1}$$

$$\frac{\partial \psi}{\partial \theta} = c_p\left(p/p_0\right)^{\kappa} \tag{A2}$$

$$\frac{D}{Dt}\left(\frac{\partial p}{\partial \theta}\right) = \frac{\partial p}{\partial \theta}\left(\nabla\cdot\mathbf{v} + \frac{\partial H}{\partial \theta}\right) \tag{A3}$$

$$H = \frac{D\theta}{Dt} \tag{A4}$$

where $\psi = c_p T + gz$, $T = \theta(p/p_0)^{\kappa}$, $p_0 = 1000$ mb, $\kappa = R/c_p$,

$\mathbf{F} = -\mathbf{i}\frac{\partial}{\partial z}\overline{u'w'} - \mathbf{j}\frac{\partial}{\partial z}\overline{v'w'}$: turbulent momentum flux stress force,

$H = -\frac{\partial}{\partial z}\overline{\theta' w'}$: turbulent diabatic heating.

The gradient Richardson number in isentropic coordinates is

$$Ri = \frac{1}{\rho\theta}\left(\frac{-\partial p}{\partial \theta}\right)\left|\frac{\partial v}{\partial \theta}\right|^{-2} \qquad \text{(A5)}$$

The diagnostic Richardson number tendency following the flow is

$$\frac{D}{Dt}\ln Ri = \frac{D}{Dt}\ln\left(\frac{-\partial p}{\partial \theta}\right) - \frac{D}{Dt}\ln\left|\frac{\partial v}{\partial \theta}\right|^2 - \frac{D}{Dt}\ln\theta - \frac{D}{Dt}\ln\rho \qquad \text{(A6)}$$

The term $D\ln\theta/Dt = 0$ in the adiabatic case. For this study, where turbulence is considered as a diabatic heat source or sink, it will not merely be dropped. The equation of state, $p = \rho RT$, gives

$$\ln\rho = \ln p - \ln T - \ln R \qquad \text{(A7)}$$

Poisson's equation gives

$$\ln T = \ln\theta + \kappa\ln p - \kappa\ln p_s$$

(A7) gives

$$\ln\rho = \ln p - \ln\theta - \kappa\ln p + \kappa\ln p_s - \ln R$$
$$= (1-\kappa)\ln p - \ln\theta + \text{const.}$$

and

$$\frac{D}{Dt}\ln\rho = \frac{1}{\gamma}\frac{D}{Dt}\ln p - \frac{D}{Dt}\ln\theta \quad , 1-\kappa = 1/\gamma$$

since $1/(\gamma p)Dp/Dt$ is considered small enough to ignore (small compressibility) for the adiabatic case giving $D\ln\rho/Dt = 0$, the same assumption will be made for the diabatic case so that

$$\frac{D}{Dt}\ln\rho = -\frac{D}{Dt}\ln\theta$$

This is a form of the Boussinesq approximation which allows density variations only due to diabatic heating. The diagnostic Richardson number tendency (from now on called DRT) becomes

$$\frac{D}{Dt}\ln Ri = \frac{D}{Dt}\ln\left(\frac{-\partial p}{\partial \theta}\right) - \frac{D}{Dt}\ln\left|\frac{\partial v}{\partial \theta}\right|^2 \qquad \text{(A8)}$$

What is needed is an expression for DRT in terms of the governing primitive equations (A1)-(A4). The turbulent stress terms will be retained in order to obtain an explicit form for the subgrid-scale DRT as well as the turbulent kinetic energy dissipation rate, .

The second right-hand-term can be obtained as follows: (A1) gives

$$\frac{\partial}{\partial t}\left(\frac{\partial \mathbf{v}}{\partial \theta}\right) + \left(\mathbf{v}\cdot\nabla\frac{\partial \Psi}{\partial \theta}\right) + H\frac{\partial}{\partial \theta}\left(\frac{\partial \mathbf{v}}{\partial \theta}\right) + \left(\frac{\partial \mathbf{v}}{\partial \theta}\cdot\nabla\right)\mathbf{v} + \frac{\partial H}{\partial \theta}\frac{\partial \mathbf{v}}{\partial \theta} = -\nabla\frac{\partial \Psi}{\partial \theta} - f\mathbf{k}\times\mathbf{v} + \frac{\partial \mathbf{F}}{\partial \theta}$$

$$\frac{D}{Dt}\left(\frac{\partial \mathbf{v}}{\partial \theta}\right) = -\left(\frac{\partial \mathbf{v}}{\partial \theta}\cdot\nabla\right)\mathbf{v} - \frac{\partial H}{\partial \theta}\frac{\partial \mathbf{v}}{\partial \theta} - \nabla\frac{\partial \Psi}{\partial \theta} - f\mathbf{k}\times\frac{\partial \mathbf{v}}{\partial \theta} + \frac{\partial \mathbf{F}}{\partial \theta} \qquad \text{(A9)}$$

$\frac{\partial \mathbf{v}}{\partial \theta}\cdot$(A9) gives

$$\frac{1}{2}\frac{D}{Dt}\left|\frac{\partial \mathbf{v}}{\partial \theta}\right|^2 = -\frac{\partial \mathbf{v}}{\partial \theta}\cdot\left(\frac{\partial \mathbf{v}}{\partial \theta}\cdot\nabla\right)\mathbf{v} - \left|\frac{\partial \mathbf{v}}{\partial \theta}\right|^2\frac{\partial H}{\partial \theta} - \frac{\partial \mathbf{v}}{\partial \theta}\cdot\nabla\frac{\partial \Psi}{\partial \theta} + \frac{\partial \mathbf{v}}{\partial \theta}\cdot\frac{\partial \mathbf{F}}{\partial \theta}$$

and

$$\frac{D}{Dt}\left|\frac{\partial \mathbf{v}}{\partial \theta}\right|^2 = -2\frac{\partial \mathbf{v}}{\partial \theta}\cdot\left(\frac{\partial \mathbf{v}}{\partial \theta}\cdot\nabla\right)\mathbf{v} - 2\left|\frac{\partial \mathbf{v}}{\partial \theta}\right|^2\frac{\partial H}{\partial \theta} - 2\frac{\partial \mathbf{v}}{\partial \theta}\cdot\nabla\frac{\partial \Psi}{\partial \theta} + 2\frac{\partial \mathbf{v}}{\partial \theta}\cdot\frac{\partial \mathbf{F}}{\partial \theta} \qquad \text{(A10)}$$

Using the hydrostatic equation (A2), and the Poisson equation,

$$\nabla\frac{\partial \Psi}{\partial \theta} = c_p\nabla\left(p/p_0\right)^{\kappa} = c_p\nabla\left(T/\theta\right) = \frac{c_p}{\theta}\nabla T$$

Eq (A10) becomes

$$\frac{D}{Dt}\left|\frac{\partial \mathbf{v}}{\partial \theta}\right|^2 = -2\frac{\partial \mathbf{v}}{\partial \theta}\cdot\left(\frac{\partial \mathbf{v}}{\partial \theta}\cdot\nabla\right)\mathbf{v} - 2\frac{c_p}{\theta}\frac{\partial \mathbf{v}}{\partial \theta}\cdot\nabla T - 2\left|\frac{\partial \mathbf{v}}{\partial \theta}\right|^2\frac{\partial H}{\partial \theta} + 2\frac{\partial \mathbf{v}}{\partial \theta}\cdot\frac{\partial \mathbf{F}}{\partial \theta}$$

and

$$\frac{D}{Dt}\ln\left|\frac{\partial \mathbf{v}}{\partial \theta}\right|^2 = -2\left|\frac{\partial \mathbf{v}}{\partial \theta}\right|^{-2}\frac{\partial \mathbf{v}}{\partial \theta}\cdot\left(\frac{\partial \mathbf{v}}{\partial \theta}\cdot\nabla\right)\mathbf{v} - 2\frac{c_p}{\theta}\left|\frac{\partial \mathbf{v}}{\partial \theta}\right|^{-2}\frac{\partial \mathbf{v}}{\partial \theta}\cdot\nabla T - 2\frac{\partial H}{\partial \theta} + 2\left|\frac{\partial \mathbf{v}}{\partial \theta}\right|^{-2}\frac{\partial \mathbf{v}}{\partial \theta}\cdot\frac{\partial \mathbf{F}}{\partial \theta}. \qquad \text{(A11)}$$

An expression for the first right-hand-side term in (A8) can be obtained directly from the continuity eq. (A3)

$$\frac{D}{Dt}\left(-\frac{\partial p}{\partial \theta}\right) = \frac{\partial p}{\partial \theta}\left(\nabla\cdot\mathbf{v} + \frac{\partial H}{\partial \theta}\right)$$

$$\frac{D}{Dt}\ln\left(-\frac{\partial p}{\partial \theta}\right) = -\nabla\cdot\mathbf{v} - \frac{\partial H}{\partial \theta} \qquad \text{(A12)}$$

The complete equation for DRT can be written, for the case when when subgrid-scale eddies and turbulence exist, as

$$\frac{D}{Dt}\ln Ri = -\Phi - \varepsilon \qquad \text{(A13)}$$

where

$$\Phi = \left\{-2\left|\frac{\partial \mathbf{v}}{\partial \theta}\right|^{-2}\left[\frac{\partial \mathbf{v}}{\partial \theta}\cdot\left(\frac{\partial \mathbf{v}}{\partial \theta}\cdot\nabla\right)\mathbf{v} + \frac{c_p}{\theta}\frac{\partial \mathbf{v}}{\partial \theta}\cdot\nabla T\right] + \nabla\cdot\mathbf{v}\right\} \qquad \text{(A14)}$$

(1) (2) (3)

is the grid-scale contribution to the diagnostic Richardson number. The second term on the rhs of (A14) corresponds to shearing deformation by the ageostrophic grid-scale motion field which causes tilting of isentropic surfaces. The first and last terms, when taken together along the "natural" coordinate of the mean flow, represent stretching deformation. When using a non-cartesian coordinate system the first term on the rhs must be evaluated using the more general form

$$(\mathbf{v}\cdot\nabla)\mathbf{v} = (\nabla\times\mathbf{v})\times\mathbf{v} + \nabla\frac{1}{2}|\mathbf{v}|^2$$

The subgrid-scale contribution is

$$\varepsilon = 2\left|\frac{\partial \mathbf{v}}{\partial \theta}\right|^{-2}\frac{\partial \mathbf{v}}{\partial \theta}\cdot\frac{\partial \mathbf{F}}{\partial \theta} - \frac{\partial H}{\partial \theta} \qquad \text{(A15)}$$

In the absence of turbulence, then, changes in Ri are entirely due to Φ.

The role of the grid-scale dynamic processes in the generation of subgrid-scale CAT is considered with respect to its role in the dissipation of total specific energy within a parcel as it moves with the flow. Consider the layer pictured below having a potential temperature thickness $\Delta\theta$ and horizontal wind speed difference through the layer of Δv.

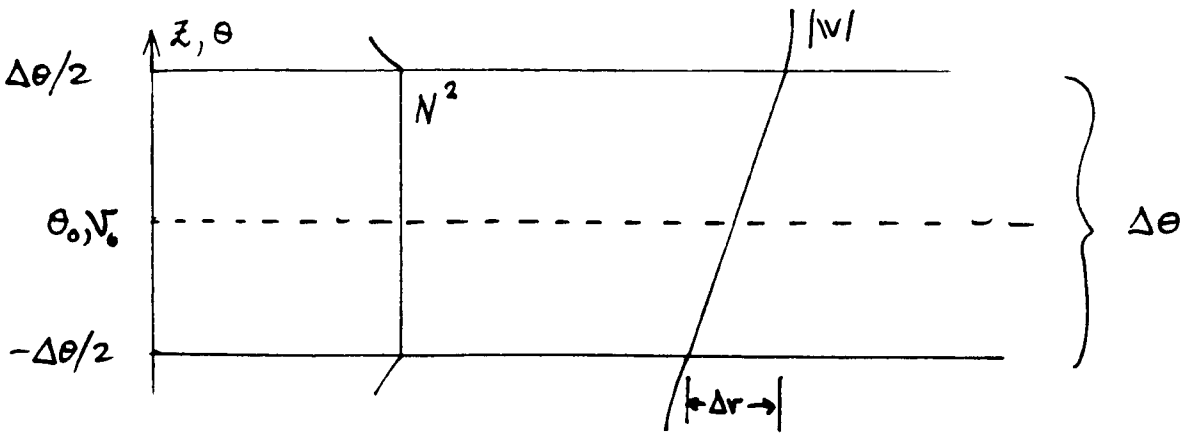

Figure A-1

The total grid-scale specific energy of the layer of "depth" $\Delta\theta$ is

$$e_L = \frac{1}{\Delta\theta}\int_{-\Delta\theta/2}^{\Delta\theta/2}\left(\frac{1}{2}w\cdot w + \gamma\right)d\theta . \qquad \text{(A16)}$$

The figure portrays a well-defined turbulent shear layer specified for the limits $\pm\Delta\theta/2$. N^2 is the Brunt-Väisälä fequency squared, a measure of the layer's static stability. In order to evaluate the integral in (A16) the structures of v and γ in the vertical direction shall be approximated by a simple linear variation. The author has evaluated this integral using a hyperbolic tangent structure for v. This exercise yielded virtually the same result as that which will be shown using the linear profiles.

For $|w|^2$

$$|w| \doteq V_0 + \frac{\Delta V}{\Delta\theta}\theta \;,\; \frac{\Delta V}{\Delta\theta} = \sqrt{\left(\frac{\partial u}{\partial\theta}\right)^2 + \left(\frac{\partial v}{\partial\theta}\right)^2} \;,\; |w_0| = V_0$$

$$\frac{1}{2}|w|^2 = \frac{1}{2}V_0^2 + \frac{\Delta V}{\Delta\theta}V_0\theta + \frac{1}{2}\left(\frac{\Delta V}{\Delta\theta}\right)^2\theta^2$$

$$\frac{1}{\Delta\theta}\int_{-\Delta\theta/2}^{\Delta\theta/2}\frac{1}{2}|w|^2 d\theta = \frac{1}{\Delta\theta}\left[\frac{1}{2}V_0^2\int d\theta + \frac{\Delta V}{\Delta\theta}V_0\int\theta\, d\theta + \frac{1}{2}\left(\frac{\Delta V}{\Delta\theta}\right)^2\int\theta^2 d\theta\right.$$

$$= \frac{1}{2}V_0^2 + \frac{1}{\Delta\theta}\,\frac{1}{2}\cdot\frac{1}{3}\left(\frac{\Delta V}{\Delta\theta}\right)^2\theta^3\Big|_{-\Delta\theta/2}^{\Delta\theta/2}$$

$$\frac{1}{\Delta\theta}\int_{-\Delta\theta/2}^{\Delta\theta/2}\frac{1}{2}|v|^2 d\theta = \frac{1}{2}v_0^2 + \frac{1}{24}(\Delta v)^2 \qquad \text{(A17)}$$

For ψ, let

$$\psi = \psi_0 + \frac{\partial \psi}{\partial \theta}\theta$$

and using the hydrostatic equation (A2) gives

$$\psi = \psi_0 + c_p\theta(p/p_0)^{\kappa} = \psi_0 + c_p T. \qquad \text{(A18)}$$

Poisson's equation, $T = \theta(p/p_0)^{\kappa}$

$$\ln T = \ln\theta + \kappa \ln p + \kappa \ln p_0$$

$$\frac{\partial}{\partial\theta}\ln T = \frac{\partial}{\partial\theta}\ln\theta + \kappa\frac{\partial}{\partial\theta}\ln p$$

$$\frac{1}{T}\frac{\partial T}{\partial\theta} = \frac{1}{\theta} + \frac{R}{c_p}\frac{1}{p}\frac{\partial p}{\partial\theta}$$

$$c_p\frac{\partial T}{\partial\theta} = c_p T/\theta - \frac{RT}{p}\left(\frac{-\partial p}{\partial\theta}\right) = c_p T/\theta - \theta\left|\frac{\partial v}{\partial\theta}\right|^2 Ri$$

$$c_p T = c_p\theta\frac{\partial T}{\partial\theta} + \left|\frac{\partial v}{\partial\theta}\right|^2\theta^2 Ri$$

so that (A18) becomes

$$\psi = \psi_0 + c_p\frac{\partial T}{\partial\theta}\theta + Ri\left|\frac{\partial v}{\partial\theta}\right|^2\theta^2$$

and $$\frac{1}{\Delta\theta}\int_{-\Delta\theta/2}^{\Delta\theta/2}\psi\, d\theta = \frac{1}{\Delta\theta}\left[\int\psi_0 d\theta + c_p\int\frac{\partial T}{\partial\theta}\theta\, d\theta + \int Ri\left|\frac{\partial v}{\partial\theta}\right|^2\theta^2 d\theta\right]$$

$$\int \frac{\partial T}{\partial \theta}\theta\, d\theta = \frac{\Delta T}{\Delta\theta}\int \theta\, d\theta = 0,$$

$$\frac{1}{\Delta\theta}\int Ri\left|\frac{\partial v}{\partial \theta}\right|^2\theta^2 d\theta = \left(\frac{\Delta v}{\Delta\theta}\right)^2\frac{Ri_L}{\Delta\theta}\int\theta^2 d\theta = \frac{-1}{12}Ri_L(\Delta v)^2$$

where $Ri_L = \int Ri\, d\theta = \frac{RT_0}{p_0\theta_0}\frac{\Delta p}{\Delta\theta}\left(\frac{\Delta v}{\Delta\theta}\right)^{-2}$: local gradient Richardson number, so that

$$\frac{1}{\Delta\theta}\int_{-\Delta\theta/2}^{\Delta\theta/2}\psi\, d\theta = \psi_0 - \frac{(\Delta v)^2}{12}Ri_L \qquad \text{(A19)}$$

Finally, (A16) becomes

$$e_L = \frac{1}{2}v_0^2 + \psi_0 + \frac{(\Delta v)^2}{24}(1-2Ri_L \qquad \text{(A20)}$$

Now it is necessary to determine the change in e_L following the parcel motion at the center of the layer. The depth of the layer $\Delta\theta$ will be kept constant. Although this means that Δp, and hence the mass of the air volume, will not remain strictly constant it will be assumed that it will not alter the basic result. The rate of change of e_L can be separated into the following components.

$$\left(\frac{D}{Dt}\right)_0 e_L = \left(\frac{D}{Dt}\right)_0\left(\frac{1}{2}v_0^2 + \psi_0\right) + \qquad \text{(A21a)}$$

$$+\left(\frac{D}{Dt}\right)_0\left[\frac{(\Delta v)^2}{24}(1-2Ri_L)\right] \qquad \text{(A21b)}$$

where the subscript 'o' ,as before, refers to quantities at the center of the layer.

The first component contributing to De /Dt is

$$\left(\frac{D}{Dt}\right)_0\left(\frac{1}{2}v_0^2 + \psi_0\right) = \frac{\partial \psi_0}{\partial t} + v_0\cdot F_0 + c_p\frac{T_0}{\theta_0}H_0 \qquad \text{(A22)}$$

The right-hand-side of (A22) is zero for steady, nonturbulent flow. Of course, this may not be assumed for this situation. However, (A22) relates to the changes in e_L at the center of the layer. It will be assumed that at the center of the layer the turbulent heat and momentum fluxes are at a maximum, so that

$$F_0 = -i\left(\frac{\partial}{\partial z}\overline{u'w'}\right)_0 - j\left(\frac{\partial}{\partial z}\overline{v'w'}\right)_0 \simeq 0$$

and

$$H_0 = -\left(\frac{\partial}{\partial z}\overline{\theta' w'}\right)_0 \simeq 0$$

The second component of $(De_L/Dt)_0$ involves the transfer of energy from the grid-scale deformation field to subgrid-scale eddies and turbulence. Equation (A21b) may be rewritten

$$\left(\frac{D}{Dt}\right)_0\left[\frac{(\Delta v)^2}{24}(1-2Ri_L)\right] = \frac{1}{12}\left[\frac{1}{2}\left(\frac{D}{Dt}\right)_0(\Delta v)^2 - Ri_L\left(\frac{D}{Dt}\right)_0(\Delta v)^2 - (\Delta v)^2\left(\frac{D}{Dt}\right)_0 Ri_L\right] \qquad \text{(A23)}$$

For DRT,

$$\left(\frac{D}{Dt}\right)_0 \ln Ri_L = \frac{1}{\Delta\theta}\int_{-\Delta\theta/2}^{\Delta\theta/2}\left(\frac{D}{Dt}\right)_0 \ln Ri \, d\theta$$

and (A13) becomes

$$\left(\frac{D}{Dt}\right)_0 \ln Ri_L = \frac{-1}{\Delta\theta}\int \underline{\Phi}\, d\theta - \frac{1}{\Delta\theta}\int \xi\, d\theta$$

$$\left(\frac{D}{Dt}\right)_0 \ln Ri_L = -\underline{\Phi}_L - \xi_L \qquad \text{(A24)}$$

Equation (A11) gives

$$\left(\frac{D}{Dt}\right)_0 \ln\left|\frac{\partial v}{\partial\theta}\right|^2 = -2\left|\frac{\partial v}{\partial\theta}\right|^{-2}\left[\frac{\partial v}{\partial\theta}\cdot\left(\frac{\partial v}{\partial\theta}\cdot\nabla\right)v + \frac{c_p}{\theta}\frac{\partial v}{\partial\theta}\cdot\nabla T\right] + 2\left|\frac{\partial v}{\partial\theta}\right|^{-2}\frac{\partial v}{\partial\theta}\cdot\frac{\partial F}{\partial\theta} - 2\frac{\partial H}{\partial\theta}$$

$$= \Phi - \nabla\cdot w + 2\left|\frac{\partial w}{\partial\theta}\right|\frac{\partial^2 w}{\partial\theta^2}\cdot\frac{\partial F}{\partial\theta} - 2\frac{\partial H}{\partial\theta}$$

$$\frac{D}{Dt}\left|\frac{\partial w}{\partial\theta}\right|^2 = \left|\frac{\partial w}{\partial\theta}\right|^2\left[\Phi - \nabla\cdot w + 2\left|\frac{\partial w}{\partial\theta}\right|^{-2}\frac{\partial w}{\partial\theta}\cdot\frac{\partial F}{\partial\theta} - 2\frac{\partial H}{\partial\theta}\right]$$

$$\frac{D}{Dt}(\Delta r)^2 = (\Delta\theta)^2\left[\frac{1}{\Delta\theta}\int\frac{D}{Dt}\left|\frac{\partial w}{\partial\theta}\right|^2 d\theta\right]$$

$$= (\Delta\theta)^2\left[\frac{1}{\Delta\theta}\int\left|\frac{\partial w}{\partial\theta}\right|^2\left(\Phi - \nabla\cdot w + 2\left|\frac{\partial w}{\partial\theta}\right|^{-2}\frac{\partial w}{\partial\theta}\cdot\frac{\partial F}{\partial\theta} - 2\frac{\partial H}{\partial\theta}\right)d\theta\right]$$

$$= (\Delta r)^2\left[\Phi_L - \nabla\cdot w_0 + \frac{2}{\Delta\theta}\left(\frac{\Delta r}{\Delta\theta}\right)^{-2}\int\frac{\partial w}{\partial\theta}\cdot\frac{\partial F}{\partial\theta}d\theta - \frac{2}{\Delta\theta}\int\frac{\partial H}{\partial\theta}d\theta\right]$$

$$\frac{1}{2}\left(\frac{D}{Dt}\right)_0(\Delta r)^2 = (\Delta r)^2\left[\frac{1}{2}\Phi_L - \frac{1}{2}\nabla\cdot w_0 + \frac{1}{\Delta\theta}\left(\frac{\Delta r}{\Delta\theta}\right)^{-2}\int\frac{\partial w}{\partial\theta}\cdot\frac{\partial F}{\partial\theta}d\theta - \frac{1}{\Delta\theta}\int\frac{\partial H}{\partial\theta}d\theta\right] \quad \text{(A25)}$$

where $\frac{1}{\Delta\theta}\int\nabla\cdot w\,d\theta = \nabla\cdot w_0$ was used. Then

$$-Ri_L\frac{D}{Dt}(\Delta r)^2 = \left[-Ri_L\Phi_L + Ri_L\nabla\cdot w_0 - Ri_L\frac{2}{\Delta\theta}\left(\frac{\Delta r}{\Delta\theta}\right)^{-2}\int_{-\Delta\theta/2}^{\Delta\theta/2}\frac{\partial w}{\partial\theta}\cdot\frac{\partial F}{\partial\theta}d\theta + Ri_L\frac{2}{\Delta\theta}\left[\int_{-\Delta\theta/2}^{\Delta\theta/2}\frac{\partial H}{\partial\theta}d\theta\right]\right] \quad \text{(A26)}$$

and from (A24), with

$$-(\Delta r)^2\frac{D}{Dt}Ri_L = (\Delta r)^2\left[Ri_L\Phi_L + Ri_L\frac{2}{\Delta\theta}\left(\frac{\Delta r}{\Delta\theta}\right)^{-2}\int_{-\Delta\theta/2}^{\Delta\theta/2}\frac{\partial w}{\partial\theta}\cdot\frac{\partial F}{\partial\theta}d\theta - Ri_L\frac{1}{\Delta\theta}\left[\int_{-\Delta\theta/2}^{\Delta\theta/2}\frac{\partial H}{\partial\theta}d\theta\right]\right] \quad \text{(A27)}$$

The final expression for (A21) can now be written

$$\left(\frac{D}{Dt}\right)_0 e_L = \frac{\partial \gamma_0}{\partial t} + \frac{(\Delta v)^2}{24}(2Ri_L - 1)\nabla\cdot V_0 + \frac{(\Delta v)^2}{24}\underline{\Phi}_L - \varepsilon_L \qquad \text{(A28)}$$

where, in terms of the subgrid-scale eddy fluxes,

$$\varepsilon_L = \frac{-(\Delta v)^2}{24}\left[\left(\frac{\Delta v}{\Delta\theta}\right)^{-2}\frac{1}{\Delta\theta}\int_{-\Delta\theta/2}^{\Delta\theta/2}\frac{\partial v}{\partial\theta}\cdot\frac{\partial F}{\partial\theta}d\theta + (Ri_L - 1)\frac{1}{\Delta\theta}\int_{}^{\Delta\theta}\frac{\partial H}{\partial\theta}d\theta\right] \qquad \text{(A29)}$$

can be considered the "explicit" form of the total energy dissipation rate. The total specific energy, from (A20), can be written

$$e_L = \frac{1}{2}V_0^2 + \gamma_0 - \frac{(\Delta v)^2}{24}(2Ri_L - 1) \qquad \text{(A30)}$$

Focusing on the last three rhs terms in (A28), which involve the actual transfer of energy from the deformation field to turbulence, in order for Ri_L to remain at a constant (and presumably small) value requires a balance between the last two terms such that

$$\varepsilon_L = \begin{cases} \dfrac{(\Delta v)^2}{24}\underline{\Phi}_L\,, & \underline{\Phi}_L > 0 \\ 0\,, & \underline{\Phi}_L \le 0 \end{cases} \qquad \text{(A31)}$$

If (A31) were not true (at least for established CAT layers), that part not balanced would act to change Ri_L. As mentioned in the main text, observations (Kennedy and Shappiro, 1975) suggest that the balance implied by (A31) may be a reasonable assumption.

II. The Diagnostic Richardson Number Tendency: Grid-scale and Subgrid-scale Effects

It should be emphasized that (A31) is strictly relevant only once the layer pictured by Figure A-1 has already become turbulent. Consider the general situation. Parcels will pass through regions where large-scale processes are acting to increase Ri_L, $\underline{\Phi}_L < 0$ and hence no turbulence, and then back into regions where the reverse is true: $\underline{\Phi}_L > 0$, and turbulence may form if Ri_L reaches Ri_{cr}. The general equation governing changes in Ri_L for a parcel is Eq. (A4) of the main text or, again,

$$\left(\frac{D}{Dt}\right)_0 \ln Ri_L = \begin{cases} -\underline{\Phi}_L & \text{, no CAT} \quad \text{(A32a)} \\ -\underline{\Phi}_L - \underline{\varepsilon}_L & \text{, CAT} \quad \text{(A32b)} \end{cases}$$

A separate equation governs the change in Ri_L, following the motion at the the center of the layer, depending on whether or not CAT has formed. Bosart and Garcia (1974) were able, of course, to use only (A32a) to calculate changes in Ri_L following the flow.

The explicit form of the DRT for the turbulent case (A32b) can be derived using the explicit forms of ε_L and $\underline{\varepsilon}_L$ from (A31) and (A15), respectively. Thus,

$$\left(\frac{D}{Dt}\right)_0 \ln Ri_L = -\underline{\Phi}_L - \underline{\varepsilon}_L$$

or

$$\frac{(\Delta v)^2}{24}\left(\frac{D}{Dt}\right)_0 \ln Ri_L = -\varepsilon_L - \frac{(\Delta v)^2}{24}\underline{\varepsilon}_L$$

so that

$$\left(\frac{D}{Dt}\right)_0 \ln Ri_L = \left(2Ri_L - 1\right)\frac{1}{\Delta\theta}\int_{-\Delta\theta/2}^{\Delta\theta/2} \frac{\partial H}{\partial\theta}\, d\theta \qquad \text{(A33)}$$

Within the layer,

$$\int \frac{\partial H}{\partial\theta}\, d\theta \begin{cases} = 0, \text{ no CAT} & \text{(A34a)} \\ < 0, \text{ CAT.} & \text{(A34b)} \end{cases}$$

Considering a turbulent sublayer which forms, dissipates and then reforms at least several times per hour, when averaging over a meso-scale time period (A34b) is the appropriate form. This means that for time scales significantly greater than those normally associated with the CAT mechanism, it can be seen from (A33) that Ri_L will be maintained at a value of 1/2.

1. REPORT NO.	2. GOVERNMENT ACCESSION NO.	3. RECIPIENT'S CATALOG NO.
NASA CR-3971		

4. TITLE AND SUBTITLE	5. REPORT DATE
The Physical and Empirical Basis for a Specific Clear-Air Turbulence Risk Index	April 1986
	6. PERFORMING ORGANIZATION CODE
7. AUTHOR(S)	8. PERFORMING ORGANIZATION REPORT #
John L. Keller	
9. PERFORMING ORGANIZATION NAME AND ADDRESS	10. WORK UNIT NO.
University of Dayton Research Institute 300 College Park Dayton, Ohio 45469	M- 522
	11. CONTRACT OR GRANT NO.
	NAS8-34687
	13. TYPE OF REPORT & PERIOD COVERED
12. SPONSORING AGENCY NAME AND ADDRESS	Contractor Report July 2, 1982 - August 30, 1985
National Aeronautics and Space Administration Washington, D.C. 20546	14. SPONSORING AGENCY CODE

15. SUPPLEMENTARY NOTES

Technical Monitors: Dennis W. Camp (retired) and Margaret B. Alexander. Prepared for the Atmospheric Sciences Division, Systems Dynamics Laboratory, Marshall Space Flight Center, Alabama 35812. Final Report.

16. ABSTRACT

The fundamental emphasis of this research was to develop a technique which would be a significant improvement over those currently used for flight planning to avoid clear air turbulence (CAT). The technique should, ideally, be both quantitative in determining potential intensity and specific in locating regions of relatively high risk. Furthermore, it should not rely on specialized data but be functional using the currently available rawinsonde observation (raob) system. Encouraging results documented in an earlier investigation were considered compelling enough to warrant a closer look into the possibilities of a Specific Clear Air Turbulence Risk (SCATR) index approach to the clear air turbulence problem. Unlike that research, which considered sustained periods of flight in light to moderate clear air turbulence, this study focuses on several cases of documented severe CAT. Results of these case studies suggest that a SCATR index is not an unrealizable goal and that uses of such an index, even in its current prototype level of development, are also apparent.

17. KEY WORDS	18. DISTRIBUTION STATEMENT
Clear Air Turbulence Specific Clear Air Turbulence Risk Wind Shear Aviation Safety	Unclassified – Unlimited STAR Category: 47

19. SECURITY CLASSIF. (of this report)	20. SECURITY CLASSIF. (of this page)	21. NO. OF PAGES	22. PRICE
Unclassified	Unclassified	47	A03

For sale by National Technical Information Service, Springfield, Virginia 22161
NASA-Langley, 1986